Crossover in the pressure evolution of elementary distortions in RFeO$_3$ perovskites and its impact on their phase transition

R. Vilarinho,[1,*] P. Bouvier,[2] M. Guennou,[3,4] I. Peral,[3,4] M. C. Weber,[3,4,5] P. Tavares,[6] M. Mihalik, Jr.,[7] M. Mihalik,[7] G. Garbarino,[8] M. Mezouar,[8] J. Kreisel,[3,4] A. Almeida,[1] and J. Agostinho Moreira[1,†]

[1]*IFIMUP, Physics and Astronomy Department, Faculty of Sciences, University of Porto, Rua do Campo Alegre 687, s/n- 4169-007 Porto, Portugal*

[2]*Université Grenoble-Alpes, CNRS, Institut Néel, 38000 Grenoble, France*

[3]*Materials Research and Technology Department, Luxembourg Institute of Science and Technology, 41 rue du Brill, L-4422 Belvaux, Luxembourg*

[4]*Physics and Materials Science Research Unit, University of Luxembourg, 162a avenue de la Faïencerie, 1511 Luxembourg, Luxembourg*

[5]*Department of Materials, ETH Zurich, Vladimir-Prelog-Weg 4, 8093 Zurich, Switzerland*

[6]*Centro de Química – Vila Real, Departamento de Química, Universidade de Trás-os-Montes e Alto Douro, 5000–801 Vila Real, Portugal*

[7]*Institute of Experimental Physics Slovak Academy of Sciences, Watsonova 47, Košice, Slovak Republic*

[8]*European Synchrotron Radiation Facility, 38043 Grenoble, France*

(Received 16 December 2018; published 25 February 2019)

This work reports on the pressure dependence of the octahedral tilts and mean Fe-O bond lengths in RFeO$_3$ (R = Nd, Sm, Eu, Gd, Tb, and Dy), determined through synchrotron x-ray diffraction and Raman scattering, and their role on the pressure-induced phase transition displayed by all of these compounds. For larger rare-earth cations (Nd-Sm), both anti- and in-phase octahedral tilting decrease as pressure increases, whereas the reverse behavior is observed for smaller ones (Gd-Dy). EuFeO$_3$ stands at the borderline, with nearly pressure-independent tilt angles. For the compounds where the tilts increase with pressure, the FeO$_6$ octahedra are compressed at lower rates than for those ones exhibiting opposite pressure tilt dependence. The crossover between the two opposite pressure behaviors is discussed in relation to the general rules proposed from different theoretical approaches. The similarity of the pressure-induced isostructural insulator-to-metal phase transition, observed in the whole series, points out that the tilts play a minor role in its driving mechanisms. A clear relationship between octahedral compressibility and critical pressure is ascertained.

DOI: 10.1103/PhysRevB.99.064109

I. INTRODUCTION

Hydrostatic pressure has been increasingly considered in the study of critical phenomena since it allows one to modify the interatomic distances and, consequently, the interactions to a greater extent than any other external parameter, such as temperature or magnetic field. Thus, the number of published experimental [1–5] and theoretical [6–13] reports concerning the pressure evolution of elementary distortions and phase transitions in many materials has steadily increased over the last few years. In this regard, the effect of hydrostatic pressure on ABO_3 perovskites has been the focus of intense research because of their remarkable pressure-induced phase transitions sequences, many of them undergoing many structural transformations accompanied by changes in their magnetic, transport, and ferroelectric properties, challenging the proposed models to explain and predict the high-pressure behavior of these compounds [1–5].

The ABO_3 perovskites exhibit a crystallographic structure that can be described as a corner-sharing BO_6 octahedra network, with the A cations placed between them, forming AO_{12} dodecahedra [14]. The structure of ABO_3 perovskites can be obtained from basic distortions of the ideal $Pm\bar{3}m$ cubic phase [15,16]. For perovskites with a tolerance factor less than unity, the most important distortion is characterized by BO_6 octahedral rotations [17]. In the case of *Pnma* orthorhombic perovskites, these distortions are in-phase and antiphase tilts about the $[010]_{pc}$ and $[101]_{pc}$ pseudocubic directions [17], which transform according to the M_3^+ and R_4^+ irreducible representations of the $Pm\bar{3}m$ space group, respectively [15,16]. These two distortions are the primary order parameters associated with the symmetry lowering, and present the largest amplitudes, which increase as the A-cation size decreases [15]. Other non-symmetry-breaking distortions occur together with octahedral tilting, where the antiparallel motion of the A cations along the z pseudocubic direction with symmetry X_5^+ is the most relevant, as it bares the largest amplitude among the secondary distortions. Moreover, it couples to both tilts via a specific trilinear coupling term that provides an energy gain crucial to the stabilization of the *Pnma* phase [15,18].

In order to predict and explain the structural behavior of perovskites under high pressure, several rules have been proposed, based on experimental results, theoretical models, and density functional theory (DFT) calculations [7–9]. The first attempts to formulate general rules regarding the

*Corresponding author: rvsilva@fc.up.pt
†Corresponding author: jamoreir@fc.up.pt

pressure dependence of the phase sequence in perovskites were based on the octahedra tilting and on the ratios of the compressibilities (M_A/M_B) and volume (V_A/V_B) of the AO_{12} and BO_6 polyhedra [9–13]. If $M_A/M_B > 1$, a transition to a higher-symmetry phase is expected, whereas the opposite should occur if $M_A/M_B < 1$ [10]. Based on the bond-valence concept, Zhao *et al.* [9] predicted that the AO_{12} dodecahedra are expected to be significantly more compressible than the BO_6 octahedra in orthorhombic perovskites, with both *A* and *B* cations having the formal charge +3 (3:3 perovskites), as is the case for rare-earth orthoferrites ($RFeO_3$). This model also evidences the correlation between the ratio of the BO_6 and AO_{12} compressibilities and the rate of change of the octahedral tilting [9]. Thus, the octahedral tilts should decrease with increasing pressure [9]. Moreover, the decrease of the octahedral tilting with pressure should yield a structural phase transition from the orthorhombic into a higher-symmetric structure at some critical pressure [9]. As a matter of fact, these rules are not followed by many of 3:3 perovskites. For instance, new results in rare-earth chromites ($RCrO_3$), with small *R* cations, show that octahedral tilting increases with pressure [19,20]. The other approach, based on the pressure evolution of the V_A/V_B ratio, followed the work of Thomas *et al.* [12], which stated that in the case of 3:3 perovskites, the V_A/V_B is equal to 5 for the ideal symmetry ($Pm\bar{3}m$) and a reduction in V_A/V_B to 4.7 is associated with a change to orthorhombic symmetry (*Pnma)*, found to be stable for V_A/V_B values down to 3.8 [12,13,21].

In order to unravel the mechanisms underlying the distinct pressure dependences of octahedral tilting, Xiang *et al.* [7] conducted first-principles calculations on representative perovskites and proposed a set of rules governing the tilt evolution with pressure. In this framework, they simulated the pressure dependence of both in-phase and antiphase octahedral tilts of $LaFeO_3$ and $LuFeO_3$, as border cases in the rare-earth orthoferrites series [7]. For $LaFeO_3$, it was found that both octahedral tilts are suppressed as pressure increases, in agreement with Zhao's prevision [7]. However, pressure suppresses the antiphase but enhances the in-phase tilting in $LuFeO_3$ [7]. This pressure behavior was interpreted by taking into account the contribution of a trilinear coupling between these two rotations and the antipolar mode involving the *A* cation [7,18]. Thus, a new rule emerges for the orthorhombic *Pnma* perovskites, which simultaneously exhibit the in-phase and antiphase octahedral tilts, stating that they are not inevitably both suppressed or enhanced by pressure [7]. Where and how the crossover between the two aforementioned distinct pressure behaviors occurs in the rare-earth orthoferrites still remains to be understood.

Despite the intensive research already done [20,22–26], a systematic study of the pressure evolution of the elementary structural distortions in orthorhombic perovskites is still missing, as well as the search for crossover events. In this regard, the study of the $RFeO_3$ series under high pressure is particularly interesting, as it is expected to show different pressure dependences of the elementary distortions across the series [7,8]. Moreover, this system bears a distinct advantage, as it does not show distortions other than those with direct origin in octahedral tilting, such as Jahn-Teller distortion, which can influence the mean *B*-O bond length [2].

In this work, we present an experimental study of the structure of the $RFeO_3$ (R = Nd, Sm, Eu, Gd, Tb, and Dy) as a function of pressure, by means of synchrotron x-ray diffraction and Raman scattering. We first analyze the pressure evolution of the octahedral tilt angles across the series in order to reach an overall picture of its dependence on the rare-earth cation size. Then, the pressure variation of the mean Fe-O bond length obtained by Raman scattering is explored in order to correlate the pressure tilt behavior and the mechanisms to accommodate pressure. We also discuss the experimental results within the scope of the predictions of theoretical models. Finally, the dependence of the critical pressure on the rare-earth cation size is examined in terms of the pressure behavior of the elementary distortions.

II. EXPERIMENTAL ASPECTS

$SmFeO_3$ single crystals were grown in an optical-floating-zone furnace [27], and $NdFeO_3$ and $TbFeO_3$ powder was prepared using single crystals grown by the floating-zone method in a FZ-T-4000 (Crystal Systems Corp.) mirror furnace. $EuFeO_3$ powder was obtained by conventional solid-state reactions, while $GdFeO_3$ and $DyFeO_3$ powder was prepared using the urea sol-gel combustion method [28]. The quality of the samples was previously characterized by means of x-ray diffraction, Fourier transform infrared spectroscopy, x-ray photoemission spectroscopy, and scanning electron microscopy. The ceramics were manually grinded to acquire a homogeneous powder and loaded in a diamond anvil cell (DAC) with diamond culets of 300 μm diameter, using a stainless-steel gasket and with helium as a pressure-transmitting medium. The pressure was monitored through the standard fluorescence method of a ruby loaded next to the sample [29]. High-pressure synchrotron x-ray diffraction (XRD) experiments on $SmFeO_3$ and $TbFeO_3$ were performed at the European Synchrotron Radiation Facility (ESRF) on the ID27 high-pressure beam line ($\lambda = 0.3738$ Å). The diffraction data were analyzed by Le Bail and Amplimodes refinements using both FULLPROF and JANA2006 software [30,31]. The Raman spectra were recorded on a Horiba LabRam at MINATEC (Grenoble, France) using a He-Ne laser at 633 nm for $TbFeO_3$ and on a Horiba T64000 spectrometer at Institut Néel (Grenoble, France) using an Ar+ laser at 514.5 nm for $RFeO_3$ (R = Nd, Sm, Eu, Gd, and Dy). In both cases, the laser power was kept below 8 mW on the DAC to avoid sample heating. Raman spectra were fitted by a sum of independent damped oscillators using IGORPRO software.

III. RESULTS

A. High-pressure XRD: $SmFeO_3$ and $TbFeO_3$

Figure 1 shows the pressure dependence of the pseudocubic lattice parameters $a_{pc} = a/\sqrt{2}$, $b_{pc} = b/2$, and $c_{pc} = c/\sqrt{2}$ (values can be found in Table I of the Supplemental Material [32]), and the pseudocubic volume $V_{pc} = V/4$ ($Z = 1$), with V the volume of the primitive cell of the *Pnma* structure of $SmFeO_3$ and $TbFeO_3$. See Fig. S1 of the Supplemental Material [32], where representative XRD patterns of both compounds, recorded at different pressures, are shown.

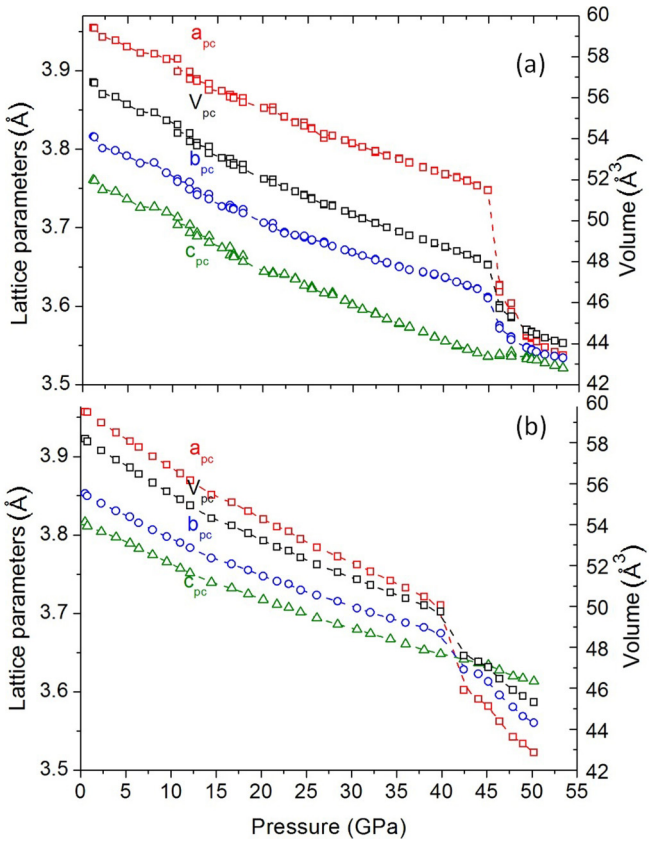

FIG. 1. Pseudocubic lattice parameters and volume as a function of pressure for (a) $TbFeO_3$ and (b) $SmFeO_3$. The dashed lines are guides for the eyes.

As the pressure increases, the pseudocubic lattice parameters monotonously decrease and suddenly down shift at around 41 GPa for $SmFeO_3$, and at 46 GPa for $TbFeO_3$; as a consequence, the pseudocubic volume is reduced 4.3% and 6.6%, respectively. The latter result gives clear evidence for a pressure-induced structural phase transition, which we will address in detail in the last section of this work. On further pressure increase, a smooth pressure evolution of the pseudocubic lattice parameters and volume is again observed. The symmetry of both the low- and high-pressure phases of $SmFeO_3$ and $TbFeO_3$ is found to be *Pnma*. This symmetry was reported for the high-pressure phase of other rare-earth orthoferrites [20,24].

In the low-pressure phase, the pressure dependence of the pseudocubic cell volume of $SmFeO_3$ and $TbFeO_3$ can be adequately described by the third-order Birch-Murnaghan isothermal equation of state [33,34],

$$P = 3B_o f_E[1+2f_E]^{5/2}\left\{1+\tfrac{3}{4}(B_o'-4)f_E\right\}, \quad (1)$$

where B_0 the bulk modulus and B_0' is its pressure derivative, all taken at room pressure, and f_E is given by

$$f_E = \frac{1}{2}\left\{\left(\frac{V_{pc}(0)}{V_{pc}}\right)^{2/3} - 1\right\}, \quad (2)$$

where V_{pc} is the pseudocubic volume at the pressure P, and $V_{pc}(0)$ is its room pressure value. Figure S2 of the Supplemental Material [32] shows the best fit of Eq. (1) to the experimental data. Table I presents the values of B_0 and B_0', obtained from the fit procedure. For both compounds, the values of the bulk modulus are not much different, taking values around 182 GPa, while the B_0' is about 4, typical of nearly isotropic compressions.

TABLE I. Pseudocubic volume at room pressure $V_{pc}(0)$, bulk modulus B_o, and its first pressure derivative B_0', obtained from the best fit of the third-order Birch-Murnaghan equation of state [Eq. (1)] to the pseudocubic volume of $TbFeO_3$ and $SmFeO_3$.

	$V_{pc}(0)$(Å^3)	B_o (GPa)	B_0'
$SmFeO_3$	58.3 ± 0.1	183 ± 3	4.0 ± 0.2
$TbFeO_3$	57.2 ± 0.1	181 ± 9	4.0 ± 0.6

B. Raman scattering

According to group theory, we expect 24 Raman-active vibration modes for the orthorhombic *Pnma* space group (see Ref. [3] for the symmetry of the Raman-active modes). The Raman spectra of $RFeO_3$, with R = Nd, Sm, Eu, Gd, Tb, and Dy, recorded at different applied pressures are shown in Fig. S3 of the Supplemental Material [32]. They simultaneously exhibit all Raman-active modes due to the unpolarized recording condition. A detailed mode assignment of the Raman bands and the corresponding atomic motions for rare-earth orthoferrites is presented elsewhere [3].

The Raman spectra for all the studied materials exhibit similar trends with increasing pressure: Raman bands shift towards higher wave numbers due to an overall pressure-induced bond shortening and volume reduction, and become broader; their intensity reduces and disappears above a certain pressure that depends on the compound. The latter result corroborates the existence of a structural phase transition at high pressures for all the studied compounds. The nature and structure of the high-pressure phase will be discussed in the last section.

In the following, we focus our attention on the Raman-active modes assigned to the FeO_6 octahedral rotations, mirroring the antiphase and in-phase octahedral tilts. Figure 2 presents the pressure dependence of the wave number of the aforementioned Raman modes of the studied compounds. The pressure dependence of the wave number of the Raman modes does not exhibit anomalous behavior up to the critical pressure, corroborating that the *Pnma* structure is preserved in the low-pressure range. A linear pressure dependence of the wave number of the Raman bands is observed below to 20 GPa. Concerning $NdFeO_3$, our results agree with those already reported below 11 GPa [26]. From the best fit of a linear function to the experimental data below to 20 GPa, shown in Fig. 2, we have determined the corresponding slopes and wave numbers at room conditions, which are presented in Table II.

The slopes of the linear pressure dependence of the wavenumber of both in-phase and antiphase tilt modes tend to increase as the rare-earth cation size decreases. We can see this result in another way: for larger tilt angles measured at

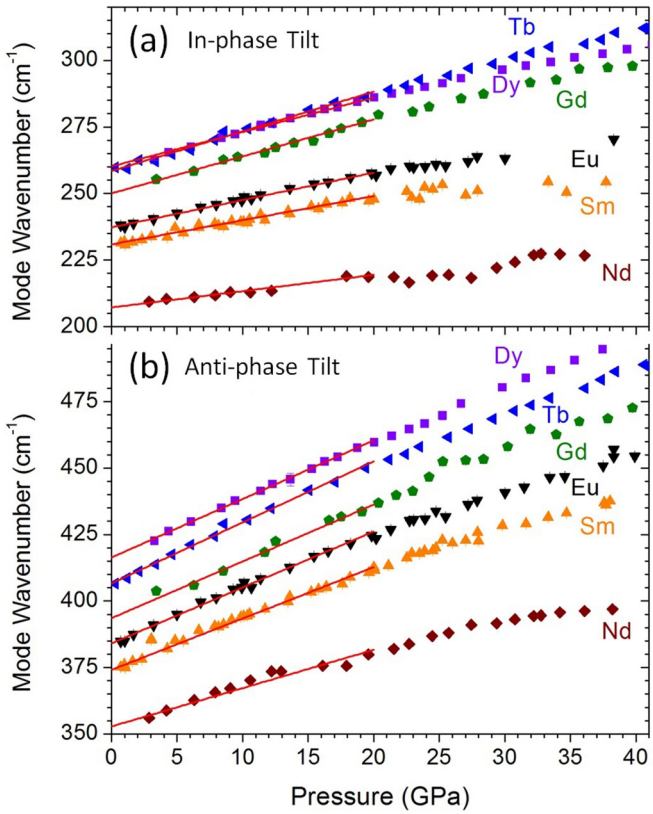

FIG. 2. Pressure evolution of the Raman modes wave number associated with (a) in-phase and (b) antiphase octahedral rotations for the different studied RFeO$_3$. The lines were obtained from the best linear fits to the data recorded below 20 GPa.

ambient pressure, greater slopes are observed, as predicted by theoretical models [7].

IV. DISCUSSION

A. Compilation and analysis of XRD data

The quality of the XRD patterns obtained at high pressures does not allow for the full Rietveld refinement of the atomic positions and, so, the calculation of the tilt angles. This is, however, possible with the AMPLIMODES analysis [15,35]. During the structure refinement, instead of allowing the atomic positions to vary in the three-dimensional space without restriction to find the global minimum, AMPLIMODES are used to improve the structure refinement by describing the displacement of the atoms, relative to their positions in the high-symmetry $Pm\bar{3}m$ structure, as the superposition of symmetry-adapted distortions [35]. The refinements show that the internal octahedral distortions have small amplitudes (less than 0.05 Å), whereas the octahedral tilts distortions and the rare-earth shifts are apparently larger (between 1 and 2 Å value of global amplitude). However, the refined mode amplitudes when plotted versus pressure show dispersion, especially in the modes mainly involving oxygen motions (that is, the tilting modes—see Fig. S4 of the Supplemental Material [32]). This is not surprising since high-pressure powder diffraction presents peak overlapping and the contribution of the oxygen atoms to the diffraction peak intensity is small compared to the rest of the atoms (that is, Sm or Tb, and Fe). The AMPLIMODES refinement results, especially regarding the octahedral tilts, should be contrasted with other observations.

TABLE II. Wave numbers at room pressure, and slopes of the linear pressure dependence of the in-phase and antiphase tilt modes, involving the data recorded below to 20 GPa.

	In-phase (cm^{-1}/Gpa)		Antiphase (cm^{-1}/Gpa)	
Compound	Wave number (cm^{-1})	Slope (cm^{-1}/Gpa)	Wave number (cm^{-1})	Slope (cm^{-1}/Gpa)
$NdFeO_3$	209.4 ± 0.8	0.43 ± 0.08	356.0 ± 0.2	1.84 ± 0.07
$SmFeO_3$	231.2 ± 0.2	0.91 ± 0.04	375.2 ± 0.2	2.10 ± 0.05
$EuFeO_3$	238.0 ± 0.1	1.10 ± 0.05	384.8 ± 0.1	2.15 ± 0.05
$GdFeO_3$	255.2 ± 0.3	1.34 ± 0.03	403.7 ± 0.3	2.04 ± 0.04
$TbFeO_3$	259.9 ± 0.4	1.53 ± 0.05	406.5 ± 0.4	2.43 ± 0.05
$DyFeO_3$	262.5 ± 0.1	1.43 ± 0.04	422.5 ± 0.1	2.28 ± 0.05

Thus, we estimated the tilt angles from the lattice parameters, using the equations of Megaw *et al.* [36,37]:

$$\theta = \cos^{-1}(a/b), \quad \varphi = \cos^{-1}(\sqrt{2}a/b), \tag{3}$$

where θ is the antiphase tilt angle around the $[101]_{pc}$ axis and φ is the in-phase tilt angle around the $[010]_{pc}$ axis. These formulas assume that the change of the unit-cell volume is originated by the octahedral tilting, with no significant additional octahedra distortion [36,37]. The formula is most suitable for larger tilts than for smaller tilts, as for the latter other contributions to the change of the unit-cell volume may be comparable to the contribution from the tilts [36,37]. Therefore, for our compounds, the estimation using Megaw's formula is better for the antiphase tilt than for the in-phase tilt, and for smaller tolerance factors than for larger ones. The reliability of this approach was assessed by comparing the values of the tilt angles for these compounds, obtained at room conditions using the Megaw's formula, with their reference ones obtained from the refinement of the atomic positions, as shown in Fig. 3. Furthermore, their pressure behaviors follow similar trends as the ones found by the AMPLIMODES analysis, though with much less dispersion (see Fig. S4 in the Supplemental Material [32]). Moreover, as we shall discuss in the following, this approach is also consistent with the pressure dependence of the spontaneous e_4 strain, calculated using the refined lattice parameters (see Fig. S5 in the Supplemental Material [32]), which is inherently connected to the two tilts [17]. The good agreement between the literature and our experimental observations ensures the validity of this method for other compounds where similar conditions are expected, such as $LuFeO_3$, $EuFeO_3$, and $NdFeO_3$. For these compounds, we have calculated the tilt angles from the lattice parameters measured at different pressures already published [20,23], as these values are relevant for the discussion of how their pressure behavior depends on the rare-earth ionic radius (see the following section).

The pressure dependence of the antiphase tilt angle for R = Nd, Sm, Eu, Tb, and Lu, and of the in-phase tilt angle for R = Sm, Eu, and Tb, are shown in Figs. 4(a) and 4(b), respectively. The data regarding the in-phase tilt angle for

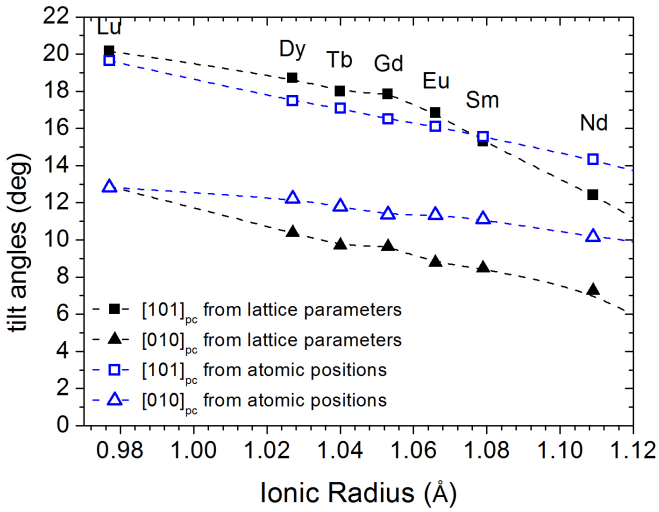

FIG. 3. Comparison of tilt angles estimated from the lattice parameters, following Eq. (3) (closed symbols), with reference values obtained from the atomic positions (open symbols). Dashed lines are guides for the eyes.

$LuFeO_3$ and $NdFeO_3$ are not presented because they are too scattered. For the same compound, both antiphase and in-phase tilt angles present similar pressure behaviors, but the pressure trend depends on the R cation. For the compounds with larger rare-earth cations ($SmFeO_3$ and $NdFeO_3$), the applied pressure causes a decrease of both antiphase and in-phase tilt angles, and thus a decrease of the values of atomic displacements associated with the symmetry-adapted R_4^+ and M_3^+ distortion modes, while the opposite behavior is observed for the compounds with smaller rare-earth cations ($LuFeO_3$ and $TbFeO_3$). A similar trend is ascertained for the pressure dependence of the spontaneous e_4 strain in the same pressure range (see Fig. S5 of the Supplemental Material [32]). The $EuFeO_3$ case sits in the transition between these two opposite pressure behaviors, where both tilt angles and, consequently, the spontaneous e_4 strain are almost pressure independent. Our experimental results point out that pressure weakens both octahedra tilts for compounds with larger rare-earth cations towards a less distorted structure, while it enhances them for compounds with smaller rare-earth cations. Moreover, a remarkable continuous evolution between the two opposite pressure behaviors is experimentally observed.

As stated by Xiang *et al.* [7], the stabilization of the *Pnma* phase in perovskites is predicted to be due to an energy gain coming from a trilinear coupling of both R_4^+ and M_3^+ distortions with the X_5^+ distortion, associated with the displacement of the rare-earth cation [8,18]. In this theoretical framework, the magnitude of the X_5^+ distortion mode is predicted to be proportional to the product of both tilt distortions [8]. If this is the case, then this distortion should follow the same trend as the tilts to which it is coupled. In fact, the pressure evolution of the X_5^+ distortion amplitude, which we have experimentally obtained by the AMPLIMODES analysis, is consistent with this model since it mimics the behavior of the tilts for the respective rare earth, as seen in Fig. 4(c).

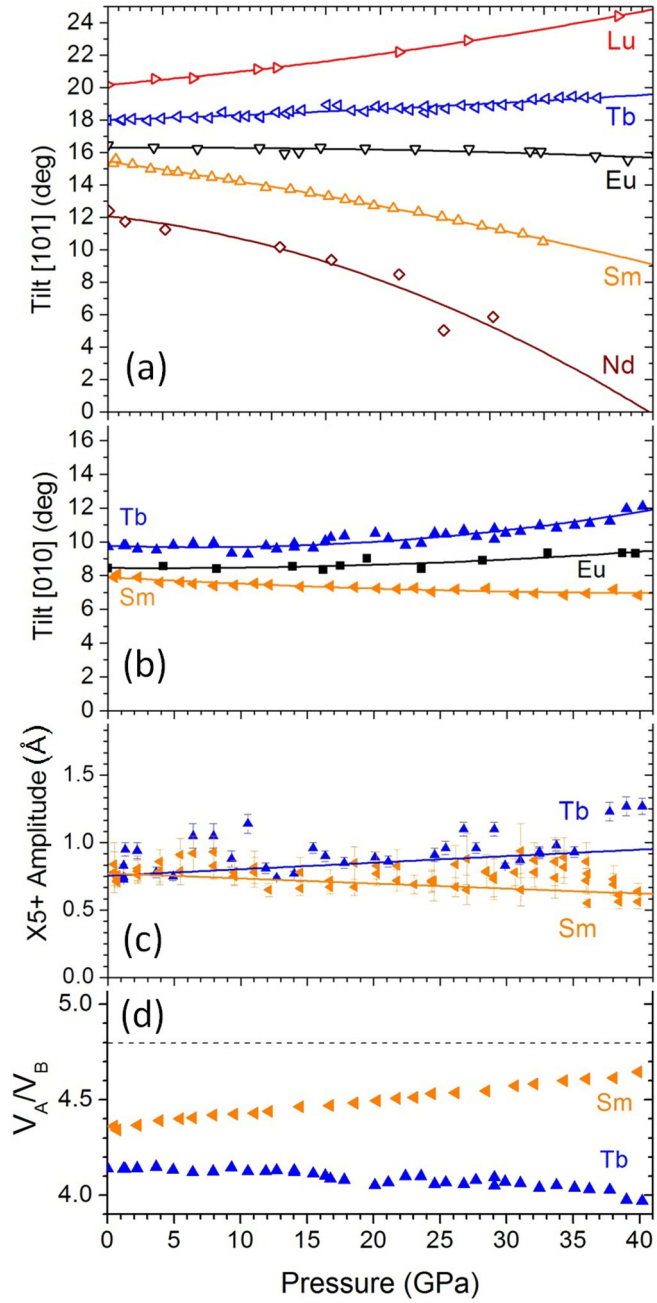

FIG. 4. Pressure dependence of the (a) antiphase and (b) in-phase octahedra tilts, calculated from the lattice parameters using the Megaw's formula, [36] for different $ReFeO_3$; (c) X_5^+ distortion calculated from AMPLIMODES refinement tool and (d) V_A/V_B ratio for $SmFeO_3$ and $TbFeO_3$ calculated following Ref. [21]. The dashed horizontal line marks the maximum value of the V_A/V_B ratio that stabilizes the *Pnma* phase [13,38]. The solid lines are guides for the eyes. Data for $LuFeO_3$ and $EuFeO_3$ from 20 and $NdFeO_3$ from 23.

B. Relation between distortion amplitudes and Raman wave numbers

Raman scattering was also used to probe the pressure dependence of both tilt angles and octahedra distortions. For the same RBO_3 system, with fixed B atom, where quite similar mean B-O bond lengths are experimentally evidenced,

a clear dependence of the tilt-mode wave numbers on the corresponding tilt angles was proposed by Iliev *et al.* [39] for orthomanganites, and more recently for rare-earth orthoferrites and orthochromites by Weber *et al.* [3,40]. However, the tilt-mode wave numbers are also dependent on the mean *B*-O bond length, as it was established by Todorov *et al.* [41], and more recently by Vilarinho *et al.* [42]. So, the tilt-mode wave numbers are functions of both the tilt angle and the *B*-O bond length. In a general approach, the wave number of the tilt mode for $R\mathrm{FeO_3}$ can be written as follows [41]:

$$\omega = (\alpha_1 - \alpha_2\langle \mathrm{Fe-O}\rangle)\varphi = (m_1 + m_2)\varphi, \tag{4}$$

where φ is the tilt angle value, $\langle \mathrm{Fe-O}\rangle$ is the mean Fe-O bond length, $\alpha_1 = 109.1\,\mathrm{cm^{-1}/deg}$, and $\alpha_2 = 42.3\,\mathrm{cm^{-1}/(Å\,deg)}$ (values taken from Ref. [41]). So, for each tilt mode, we must take into account that the slope of the pressure dependence of the corresponding wave number has two contributions: $mg_{\mathrm{total}} = m_1 + m_2$, where m_1 stands for the contribution coming from the actual tilt-angle change with pressure (α_1), and m_2 is the contribution coming from the isotropic reduction of the $\mathrm{FeO_6}$ octahedra volume; i.e., of the average Fe-O distance ($\alpha_2\langle \mathrm{Fe-O}\rangle$) [41,42]. In the following, we present an estimative of the m_2 value, and how m_1 changes with the rare-earth ionic radius, thus gaining insight on how the mean Fe-O bond length changes with pressure for each rare-earth orthoferrite.

The rare-earth cation-size dependence of the slopes of the linear pressure relation, in the 0–20 GPa range, of the Raman rotation modes, and of the antiphase and in-phase tilt angles, is depicted in Figs. 5(a) and 5(b), respectively.

The slopes of the linear pressure dependence of the Raman rotation modes, presented in Fig. 5(a), are always positive. The case of $\mathrm{EuFeO_3}$ is straightforward because the tilt angles are pressure independent, and thus $m_1 = 0$ [see Eq. (4)]. So, the linear pressure dependence of both Raman rotation modes in $\mathrm{EuFeO_3}$, observed in the 0–20 GPa range, comes from the reduction of the $\langle \mathrm{Fe-O}\rangle$ value, and $m_2 = m_{\mathrm{total}}$, which is represented by the horizontal dashed lines in Fig. 5(a). In this case, the wave number of the rotational modes mirrors the reduction of the unit-cell volume due to the decrease of the mean *B*-O bond lengths with pressure, and a linear relation between the mode wave number and volume is experimentally evidenced, as shown in Fig. 5(c) (similar plots for $\mathrm{TbFeO_3}$ and $\mathrm{SmFeO_3}$ are presented in Fig. S6 of the Supplemental Material [32] for which the linear relation does not hold, as the tilts are not constant for these compounds).

In order to unravel the effect of the tilt angles on the pressure dependence of the Raman tilt-mode wave number for the other compounds, the $m_2 = m_{\mathrm{total}}$ value calculated for $\mathrm{EuFeO_3}$ might not be the best reference since the reduction of the $\mathrm{FeO_6}$ octahedral volume may have different values for each compound, as it will be shown. According to Eq. (4), the pressure derivative of the wave number of the Raman tilt modes is

$$\frac{d\omega}{dP} = [\alpha_1 - \alpha_2\langle \mathrm{Fe-O}\rangle(P)]\frac{d\varphi}{dP} - \alpha_2\varphi(P)\left(\frac{d\langle \mathrm{Fe-O}\rangle}{dP}\right). \tag{5}$$

In the following, we shall consider the values concerning $\frac{d\omega}{dP}$ and $\frac{d\varphi}{dP}$ as the slopes obtained in the 0–20 GPa range, shown in Figs. 5(a) and 5(b), respectively. For $\mathrm{EuFeO_3}$, where $\frac{d\varphi}{dP} = 0$, we obtained $\frac{d\langle Fe-O\rangle}{dP} = -0.0031 \pm 0.0001$ Å/GPa, using either anti- or in-phase tilts. For the remaining compounds, we focus our calculation to the linear range in the vicinity of P = 0 GPa, thus taking the values of $\langle \mathrm{Fe-O}\rangle$ and φ at that point. The obtained results for the low-pressure

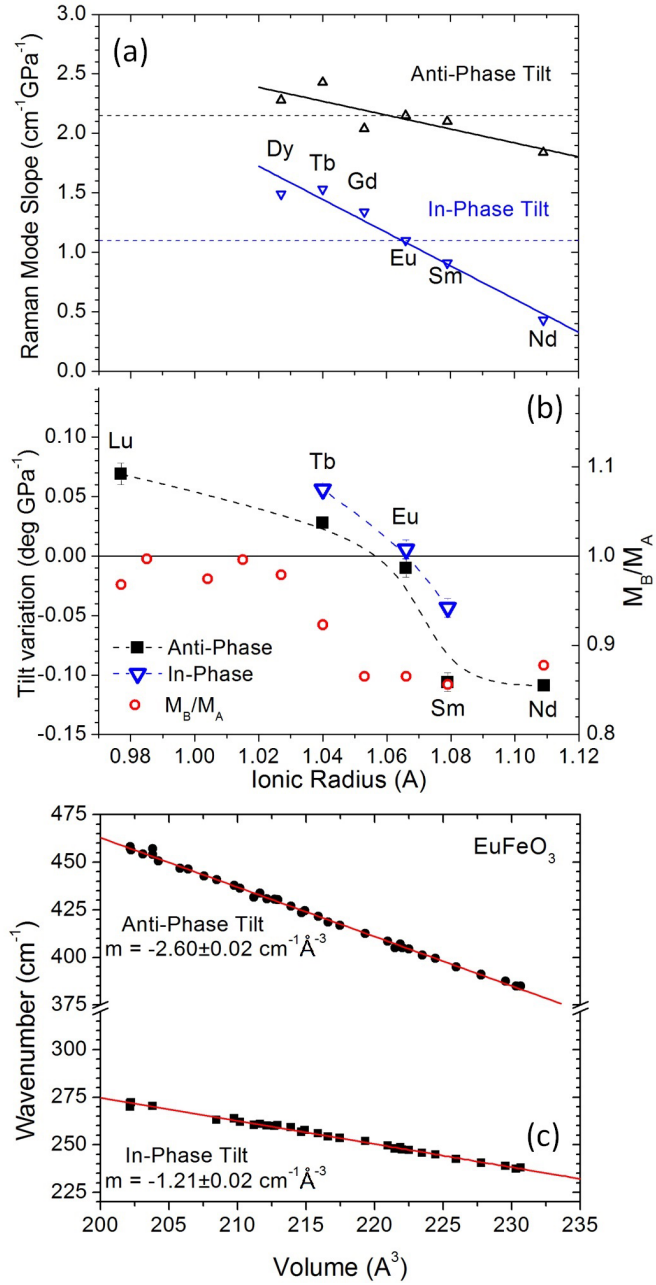

FIG. 5. Rare-earth cation-size dependence of the slopes of the linear pressure relation, in the 0–20 GPa range, of the (a) Raman rotation modes and (b) antiphase and in-phase tilt angles. (c) Volume dependence of the wave number of the Raman octahedra rotational modes for $\mathrm{EuFeO_3}$. Dashed lines in (a) mark the reference value of $\mathrm{EuFeO_3}$ for the contribution of the $\mathrm{FeO_6}$ octahedra reduction. For comparison, we also present in (b) the ratio between the compressibilities of the AO_{12} dodecahedra β_A and the $\mathrm{FeO_6}$ octahedra β_B : $\beta_A/\beta_B = M_B/M_A$, from Zhao's work [9].

TABLE III. $d\langle\text{Fe-O}\rangle/dP$ calculated from Eq. (5), for the low-pressure range, using either the anti- or the in-phase tilt angles, for the different rare-earth orthoferrites.

	$d\langle\text{Fe}-\text{O}\rangle/dP$ (Å/GPa)	
Tilt angle	Antiphase	In-phase
$TbFeO_3$	-0.0023 ± 0.0003	-0.0009 ± 0.0004
$EuFeO_3$	-0.0031 ± 0.0001	-0.0031 ± 0.0001
$SmFeO_3$	-0.0071 ± 0.0003	-0.0058 ± 0.0006
$NdFeO_3$	-0.0082 ± 0.0003	N/A

range are shown in Table III. The estimated $\frac{d\langle Fe-O\rangle}{dP}$ values varied only around 0.001 Å/GPa when using the two different rotation modes. It is worthwhile to note that Weber *et al.* [3] have found different proportionality constants (m_{total}) between ω and φ for the anti- and in-phase tilts for the $R\text{FeO}_3$ system. The presented value agrees with that obtained by Todorov *et al.* [41] for the antiphase tilt, but not for the in-phase tilt. Therefore, the most suitable value for the actual $\frac{d\langle\text{Fe}-\text{O}\rangle}{dP}$ should be the one obtained with the antiphase tilt.

These results evidence that at low pressures, as the rare-earth ionic radius increases, the pressure rate at which the FeO_6 octahedra reduce also increases. For $TbFeO_3$, the average reduction of the Fe-O mean bond length is of -0.0016 Å/GPa, which is half the value of $EuFeO_3$, and around five times smaller than the largest one of -0.0082 Å/GPa for $NdFeO_3$. This is not unexpected since the tilts provide a mechanism of pressure accommodation. Thus, for the smaller rare-earth cations, where the tilts increase with pressure, the FeO_6 octahedra are compressed at lower rates. Conversely, for the larger rare earths, where the tilts decrease with pressure, the FeO_6 octahedra are compressed at larger rates.

C. Crossover for the behavior of tilts in the rare-earth series: Experiment and theory

We now focus on the evolution of the tilt angles in the vicinity of zero (atmospheric) pressure across the series. From Fig. 5(b), we can observe that the slope of the linear pressure dependence of both antiphase and in-phase octahedral tilt angles is positive for compounds with smaller rare-earth cations (R = Lu and Tb), while they are negative for those with larger rare-earth cations (R = Sm and Nd). $EuFeO_3$ stands at the borderline, as for this compound both slopes are negligibly small. The modulus of the slope of the linear pressure dependence of the in-phase tilt angle is smaller than the antiphase tilt angle for $SmFeO_3$, while for $TbFeO_3$ it is the opposite. These results show that the way the pressure is accommodated is different for compounds with different rare-earth cationic sizes.

We now compare this compilation of experimental results with predictions made by theoretical approaches for the pressure evolution of tilt angles. A first approach is based on the compressibility of the polyhedra forming the perovskite structure. In this approach, the ratio of compressibilities β_A/β_B between the AO_{12} and BO_6 polyhedra is used as a predictor of the behavior of tilt angles under pressure, and is calculated by a valence-bond sum model: tilt angles are expected to increase when this ratio is larger than unity, and decrease otherwise. The case of the rare-earth orthoferrites has been treated in Ref. [9], and the corresponding data are reported in Fig. 5(b) for comparison. The ratio is always positive, but decreases as the ionic radius increases and reaches values very close to unity for the smallest cations [9]. According to this criterion, all compounds in the series should see their tilt angles reduced under pressure, with the exception of $TmFeO_3$ [9]. This is not what is found experimentally, but the overall evolution bears a striking resemblance with the experimental one, up to an overall shift.

More recently, in a DFT-based approach, a set of rules for the evolution of tilts under pressure was proposed [7]. In this paper, the compounds with the smallest A cations (Lu, Tm) are predicted to exhibit an unusual behavior whereby the two tilt angles behave in the opposite way with pressure: the antiphase tilts are reduced, whereas the in-phase tilts are enhanced [7]. For larger cations, both tilts behave the same way and are reduced as pressure increases. Here we find no evidence for this behavior, but instead both tilt angles behave the same in all investigate compounds. Also, Ref. [7] does not predict any case where both tilts increase under pressure.

The discrepancies between the theoretical and experimental results seemingly point to a specific difficulty in predicting the tilt behavior for the smallest cations in the series. While we cannot be conclusive at this point about the precise reasons for this discrepancy, we observe that in both approaches, the predicted tilt changes under pressure reach extremely small values, typically below 0.01°/GPa for $LuFeO_3$ in Ref. [7]. For $EuFeO_3$, which in fact has absolute pressure derivatives below 0.01°/GPa, the slopes for in-phase and antiphase tilts are of opposite sign (0.006 and -0.01°/GPa, respectively), but with values negligibly small that fall within the experimental uncertainty. In that context, it is conceivable that some additional parameters, legitimately neglected for large cations, become relevant and suffice to change the trend from slightly positive to negative, or vice versa. In particular, $R\text{FeO}_3$ with very small cations (Er-Lu) are known to exhibit some distortions of the AO_{12} polyhedra, so that the classical separation of the 12 A-O bonds into four longer bonds and eight shorter bonds becomes less satisfactory [43]. We hypothesize that this has an influence of the bond valence sum and compressibilities calculated in Ref. [7]. In the DFT approach, where calculations are performed at 0 K and the behavior of tilts is the result of a delicate balance between the pressure evolution of the Landau parameters, one might question the role of temperature effects. Differences in tilt angles of the order of 0.1° between 0 and 300 K—which is reasonable following Ref. [44]—would be equivalent to several tens of GPa and cause significant shifts in the predicted behavior. Altogether, further work will be needed to clarify the picture for small cations, which calls for detailed experimental studies and reexamination of theoretical models.

D. High-pressure phase transition

All studied compounds exhibit a phase transition at high pressure. This phase transition is clearly evidenced by the changes on the XRD patterns, mirroring the sudden changes

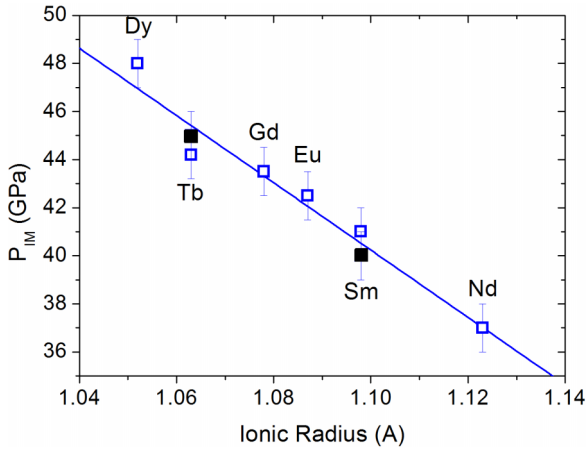

FIG. 6. Critical pressure P_{IM}, obtained from XRD (closed symbols) and Raman scattering (open symbols) data, as a function of rare-earth ionic radius.

of the pseudocubic lattice parameters. The structural phase transition reveals itself by the disappearance of the Raman signal above a certain critical pressure, hereafter designated by P_{IM}. The crystallographic structure of the high-pressure phase of $SmFeO_3$ and $TbFeO_3$ is *Pnma*, as has been reported for other rare-earth orthoferrites [20]. This structure allows for a Raman signal. Therefore, the disappearance of the Raman spectra above the critical pressure suggests the metallic character of the high-pressure structural phase. The pressure hysteresis evidenced by the XRD patterns of $SmFeO_3$ and $TbFeO_3$, and Raman spectra, for all studied compounds, recorded on increasing and decreasing pressure runs (3 to 6 GPa depending on the rare-earth cation), evidences for the first-order character of the high-pressure structural phase.

Taking into account both the XRD and Raman data, we can estimate the critical pressure P_{IM} for the studied compounds, which is depicted in Fig. 6. As can be observed, the critical pressure linearly increases as the rare-earth cation size decreases. In spite of this, all transitions are very similar in character, and it is reasonable to assume that all of them result from the same kind of high-spin to low-spin transition revealed by high-pressure Mössbauer spectroscopy [24].

It is remarkable that all the studied compounds exhibit a similar pressure-induced structural phase transition, regardless of the strong differences in their tilt evolution or their mechanisms accommodating the volume reduction. This can be first analyzed with respect to the predictors proposed to analyze the stability of the different tilted phases of perovskites. Thomas *et al.* [12], and later on Avdeev *et al.* [13], have determined that the *Pnma* phase is stable whenever V_A/V_B is smaller than 4.8. Since the V_A/V_B ratio is known to scale with the tilt angles [21,38], we have estimated its pressure dependence following the equations of Wang *et al.* [21] for $TbFeO_3$ and $SmFeO_3$. The obtained results are plotted in Fig. 4(d). For $TbFeO_3$, and for any other $RFeO_3$ where the tilt angles increase with pressure, the V_A/V_B ratio decreases with pressure and drives the crystal away from the stability limit of 4.8. On the other hand, decreasing tilts, such as in $SmFeO_3$, do drive the perovskite towards the edge of the stability range, but, in $SmFeO_3$, the high-spin to low-spin transition, which is of totally different nature and beyond the scope of the polyhedra compressibility models, occurs before this limit is actually reached. We could expect the line to be crossed for larger cations, as a result of a quicker tilt reduction. We cannot make any conclusive statement for $NdFeO_3$, but for $LaFeO_3$, a transition at 21 GPa has indeed been reported, with a change in tilts, before the high-spin to low-spin transition at 38 GPa. Altogether, we conclude that the predictors by Thomas and Avdeev remain valid under pressure, at least within the range accessible with the orthoferrites. This is also consistent with the idea that the phase transition seen in most orthoferrites has a different origin, where tilts play a minor role. We also note that the high-pressure metallic phases also seem to adopt the *Pnma* structure and it would be interesting to check whether or not those predictors, which were derived from analyses of low-pressure, insulating phases, still hold for the *metallic Pnma* perovskites with distinct electronic properties. But data are too scarce at this point and this is left for future studies.

As the tilts have little impact on this transition, it is sensible to assume that is depends mostly on the chemistry of the FeO_6 octahedra. We suggest that as pressure increases and the FeO_6 octahedra become smaller, a critical volume of the octahedron is reached where the electronic repulsion between the oxygens p electrons and the iron e_g electrons is such that it triggers this electronic reconfiguration, as it is energetically favorable for the e_g electrons to pair with the t_{2g} electrons, avoiding coming closer to the oxygen p electrons. The critical volume can be estimated for $EuFeO_3$. As the tilt angles do not change with pressure, there is an isotropic volume reduction of the unit cell, already evidenced in Fig. 5(c), and thus the ratio of the FeO_6 octahedron with the pseudocubic unit-cell volume (V_{FeO6}/V_{pc}) can be assumed to be pressure independent. Considering a regular octahedron at room pressure, the ratio $V_{FeO6}/V_{pc} = 0.189$ is obtained. Using the value of V_{pc} before the critical pressure, the critical volume for $EuFeO_3$ is estimated to be $V_{FeO6} = 9.5 \pm 0.2$ Å^3.

It is expected that for larger R cations, where from Table III we know the FeO_6 octahedra reduce their volume at a larger rate, the aforementioned phenomenon is promoted at a lower critical pressure. Conversely, for the smaller R cations, as the FeO_6 octahedra reduce their volume at a lower rate, they present higher values of critical pressure. This prediction explains the behavior of P_{IM} with the rare-earth size, shown in Fig. 6. Moreover, one can infer that a similar role is played by the octahedral tilting in the similar pressure-driven phase transition observed in $RMnO_3$ [2]. The critical pressures for $RMnO_3$ have similar dependence on the rare-earth ionic size, being always slightly higher by a constant value of 2 GPa. This difference can be assigned to the Jahn-Teller distortion present in $RMnO_3$, as it provides an additional pressure accommodation mechanism than their respective $RFeO_3$ compounds. It is worthwhile to note that the tilt angles are almost the same, thus allowing for this comparison [42]. This fact also supports the importance of the chemistry inside the octahedra in determining the symmetry of the high-pressure phase. This is because, unlike the isostructural phase transition found for the $RFeO_3$, the $RMnO_3$ present many different symmetries of the high-pressure phase [2].

V. CONCLUSIONS

In this work, we present an experimental study of the pressure dependence of the main structural distortions and lattice dynamics in the RFeO$_3$ by XRD and Raman spectroscopy. First, we have ascertained the crossover of the pressure dependence of both anti- and in-phase octahedral tilting in the RFeO$_3$ series. EuFeO$_3$ stands distinctly at the borderline, where both tilts are pressure independent. For larger rare-earth cations, we have found that the octahedral tilting decreases as pressure increases, whereas the reverse behavior is observed for smaller ones.

Furthermore, the pressure dependence of the mean Fe-O bond length, estimated from Raman data, enabled us to determine the way the pressure is accommodated in the RFeO$_3$ series. We observed that for the compounds where the tilts increase with pressure, the FeO$_6$ octahedra are compressed at lower rates than for those showing opposite pressure tilt dependence.

Finally, we determined that all the compounds of the RFeO$_3$ series undergo a pressure-induced isostructural insulator-to-metal phase transition. Thus, we have to conclude that the different pressure evolutions of the octahedral tilts play a minor role in its driving mechanisms. Moreover, we have interpreted the rare-earth ionic-size dependence of the transition pressure in terms of reaching a critical volume size of the FeO$_6$ octahedra, estimated to be $V_{\mathrm{FeO6}} = 9.5 \pm 0.2$ Å^3 in EuFeO$_3$. For the smaller R cations, as the FeO$_6$ octahedra reduce their volume at a lower rate, a shift of the transition to higher pressures occurs, contrarily to the case of larger R cations, wherein the volume increases at a higher rate.

ACKNOWLEDGMENTS

The authors thank J. Jacobs for He gas loading at ESRF (Proposal HC/2153). The authors also thank G. KH. Rozenberg and M. P. Pasternak for giving access to the details of their published XRD data concerning EuFeO$_3$ and LuFeO$_3$. The authors thank W. Ren (Shanghai University) for providing high-quality samples. The authors would like to acknowledge the support of the Projects No. Norte-070124-FEDER-000070, No. PTDC/Fis–NAN/0533/2012, and No. VEGA 2/0137/19, and R.V. for Grant No. PD/BD/114456/2016 by FCT. M.G., J.K., and M.C.W. acknowledge financial support from the Fond National de Recherche Luxembourg through a PEARL grant (FNR/P12/4853155/Kreisel).

[1] J. Oliveira, J. Agostinho Moreira, A. Almeida, V. H. Rodrigues, M. M. R. Costa, P. B. Tavares, P. Bouvier, M. Guennou, and J. Kreisel, Phys. Rev. B **85**, 052101 (2012).
[2] D. A. Mota, A. Almeida, V. H. Rodrigues, M. M. R. Costa, P. Tavares, P. Bouvier, M. Guennou, J. Kreisel, and J. A. Moreira, Phys. Rev. B **90**, 054104 (2014).
[3] M. C. Weber, M. Guennou, H. J. Zhao, J. Íñiguez, R. Vilarinho, A. Almeida, J. A. Moreira, and J. Kreisel, Phys. Rev. B **94**, 214103 (2016).
[4] T. Aoyama, K. Yamauchi, A. Iyama, S. Picozzi, K. Shimizu, and T. Kimura, Nat. Commun. **5**, 4927 (2014).
[5] T. Aoyama, A. Iyama, K. Shimizu, and T. Kimura, Phys. Rev. B **91**, 081107(R) (2015).
[6] O. E. González-Vázquez, J. C. Wojdeł, O. Diéguez, and J. Íñiguez, Phys. Rev. B **85**, 064119 (2012).
[7] H. J. Xiang, M. Guennou, J. Íñiguez, J. Kreisel, and L. Bellaiche, Phys. Rev. B **96**, 054102 (2017).
[8] P. Chen, M. N. Grisolia, H. J. Zhao, O. E. González-Vázquez, L. Bellaiche, M. Bibes, B. G. Liu, and J. Íñiguez, Phys. Rev. B **97**, 024113 (2018).
[9] J. Zhao, N. L. Ross, and R. J. Angel, Acta Crystallogr. Sect. B Struct. Sci. **60**, 263 (2004).
[10] R. J. Angel, J. Zhao, and N. L. Ross, Phys. Rev. Lett. **95**, 025503 (2005).
[11] T. Tohei, A. Kuwabara, T. Yamamoto, F. Oba, and I. Tanaka, Phys. Rev. Lett. **94**, 035502 (2005).
[12] N. W. Thomas, Acta Crystallogr. Sect. B Struct. Sci. B **52**, 954 (1996).
[13] M. Avdeev, E. N. Caspi, and S. Yakovlev, Acta Crystallogr. Sect. B Struct. Sci. **63**, 363 (2007).
[14] R. H. Mitchell, *Perovskites, Modern and Ancient* (Almaz Press, Ontario, Canada, 2002).
[15] J. M. Perez-Mato, D. Orobengoa, and M. I. Aroyo, Acta Crystallogr. Sect. A **66**, 558 (2010).
[16] M. A. Carpenter and C. J. Howard, Acta Crystallogr. Sect. B **65**, 134 (2009).
[17] A. M. Glazer, Acta Crystallogr. Sect. B **28**, 3384 (1972).
[18] N. Miao, N. C. Bristowe, B. Xu, M. J. Verstraete, and P. Ghosez, J. Phys.: Condens. Matter **26**, 035401 (2014).
[19] V. S. Bhadram, D. Swain, R. Dhanya, M. Polentarutti, A. Sundaresan, and C. Narayana, Mater. Res. Express **1**, 026111 (2014).
[20] G. K. Rozenberg, M. P. Pasternak, W. M. Xu, L. S. Dubrovinsky, S. Carlson, and R. D. Taylor, Europhys. Lett. **71**, 228 (2005).
[21] D. Wang and R. J. Angel, Acta Crystallogr. Sect. B Struct. Sci. **67**, 302 (2011).
[22] A. G. Gavriliuk, G. N. Stepanov, I. S. Lyubutin, A. S. Stepin, I. A. Trojan, and V. A. Sidorov, Hyperfine Interact. **126**, 305 (2000).
[23] A. G. Gavriliuk, I. A. Troyan, R. Boehler, M. I. Eremets, I. S. Lyubutin, and N. R. Serebryanaya, J. Exp. Theor. Phys. Lett. **77**, 619 (2003).
[24] M. P. Pasternak, W. M. Xu, G. K. Rozenberg, and R. D. Taylor, Mat. Res. Soc. Symp. Proc. **718**, D2.7.1 (2002).
[25] M. Etter, M. Müller, M. Hanfland, and R. E. Dinnebier, Acta Crystallogr. Sect. B Struct. Sci. Cryst. Eng. Mater. **70**, 452 (2014).
[26] M. Mihalik jr., M. Misek, M. Vavra, K. M. Lebecki, D. Legut, M. Mihalik, K. V. Kamenev, and M. Zentková, High Press. Res. **35**, 1 (2015).
[27] S. Cao, H. Zhao, B. Kang, J. Zhang, and W. Ren, Sci. Rep. **4**, 5960 (2014).

[28] J. Agostinho Moreira, A. Almeida, W. S. Ferreira, M. R. Chaves, J. B. Oliveira, J. M. M. da Silva, M. A. Sá, S. M. F. Vilela, and P. B. Tavares, J. Electroceram. **25**, 203 (2010).
[29] H. K. Mao, J. Xu, and P. M. Bell, J. Geophys. Res. **91**, 4673 (1986).
[30] J. Rodríguez-Carvajal, *An Introduction to the Program FullProf* (Laboratoire Leon Brillouin, CEA-CNRS, 2001).
[31] V. Petrícek, M. Dušek, and L. Palatinus, Z. Krist. **229**, 345 (2014).
[32] See Supplemental Material at http://link.aps.org/supplemental/10.1103/PhysRevB.99.064109 for XRD patterns and Raman scattering spectra, fit of the Birch-Murnaghan equation of state, distortion modes amplitude, strain and lattice parameter values with pressure, and volume dependence of Raman octahedral rotational modes.
[33] F. Birch, Phys. Rev. **71**, 809 (1947).
[34] F. Birch, J. Geophys. Res. **83**, 1257 (1978).
[35] D. Orobengoa, C. Capillas, M. I. Aroyo, and J. M. Perez-Mato, J. Appl. Crystallogr. **42**, 820 (2009).
[36] H. D. Megaw, *Crystal Structures: A Working Approach* (W. B. Saunders, Philadelphia, PA, 1973).
[37] Y. Zhao, D. J. Weidner, J. B. Parise, and D. E. Cox, Phys. Earth Planet. Inter. **76**, 1 (1993).
[38] N. W. Thomas, Acta Crystallogr. Sect. B Struct. Sci. B **52**, 16 (1996).
[39] M. N. Iliev, M. V. Abrashev, J. Laverdière, S. Jandl, M. M. Gospodinov, Y. Q. Wang, and Y. Y. Sun, Phys. Rev. B **73**, 064302 (2006).
[40] M. C. Weber, J. Kreisel, P. A. Thomas, M. Newton, K. Sardar, and R. I. Walton, Phys. Rev. B **85**, 054303 (2012).
[41] N. D. Todorov, M. V Abrashev, and V. G. Ivanov, J. Phys.: Condens. Matter **24**, 175404 (2012).
[42] R. Vilarinho, D. J. Passos, E. C. Queirós, P. B. Tavares, A. Almeida, M. C. Weber, M. Guennou, J. Kreisel, and J. A. Moreira, Phys. Rev. B **97**, 144110 (2018).
[43] M. Marezio, J. P. Remeika, and P. D. Dernier, Acta Crystallogr. Sect. B **26**, 2008 (1970).
[44] S. M. Selbach, J. R. Tolchard, A. Fossdal, and T. Grande, J. Solid State Chem. **196**, 249 (2012).